DOI: 10.13009/EUCASS2023-557
Aerospace Europe Conference 2023 – 10TH EUCASS – 9TH CEAS

Effect of nozzle seal rupture on internal motor dynamics

Laurent François⋆
⋆*ONERA - The French Aerospace Lab*
6 Chemin de la Vauve aux Granges, 91123 Palaiseau, Frace
laurent.francois@onera.fr

Abstract

Before firing, solid rocket motors are usually made airtight with a nozzle seal, designed to break at high chamber pressure to favour ignition. Once ruptured, the seal is ejected through the nozzle, a process whose characteristic time may impact the choking of the nozzle throat, as well as the pressure waves inside the chamber. In particular, it may have an important effect on the intensity of the initial expansion wave, and thus on the structural loading of the motor. All ignition simulations reported in the literature assume that the nozzle seal instantaneously disappears once its breaking pressure is reached, and no study has been reported on the effect of this nozzle seal rupture and ejection time scale. We present two approaches to model and simulate this effect. The first one assumes that the seal is ejected as a single panel and uses advanced 3D mesh handling techniques to capture its movement and interaction with the nozzle flow. The second one assumes a quasi-one-dimensional flow (Q1D) and represents the seal rupture as a gradual opening of the nozzle. This requires a novel boundary condition formulation to ensure the effect of the seal is well accounted for. We show that both approaches yield nearly identical dynamics on a small-scale test motor, thus validating the use of the more cost-effective Q1D approach. Parametric studies in Q1D show that there exists a threshold value of the characteristic rupture time below which the internal dynamics is identical to that obtained when assuming an instantaneous opening of the seal. For longer rupture times, the intensity of the expansion wave may be greatly reduced.

1. Introduction

Solid rocket motors are usually protected from the outer atmosphere via the use of a nozzle seal, which is designed to break once the chamber pressure reaches a sufficiently large value. This ensures a non-polluted internal gas composition, the absence of moisture, as well as the initial containment of the igniter gases and a rapid pressure rise, favouring ignition. When the seal breaks, the flow quickly accelerates through the nozzle and an expansion wave travels through the combustion chamber. Depending on its design, the seal may break in chunks of various sizes, and the debris may be ejected more or less quickly through the nozzle. A characteristic seal rupture time can be associated with these phenomena, which may correlate with the time required to establish a sonic flow at the nozzle throat. This may also have an effect on the system of pressure waves inside the chamber, in particular on the intensity of the initial expansion wave, and thus the mechanical loads exerted on the propellant and the motor. All ignition simulations reported in the literature, e.g. [1, 2], assume that the nozzle seal instantaneously disappears once its breaking pressure is reached, and no study has been reported on the effect of this nozzle seal rupture.

In this article, we focus on the analysis of this phenomenon. We present two approaches to model and simulate the effect of seal rupture. The first uses a 3D representation of the flow and of the nozzle seal. It is assumed that the seal is ejected as a single piece, without fragmentation. Using 3D mesh movement and overlapping techniques based on [3, 4] and implemented in the CFD toolchain Cedre from ONERA [5], the mesh is dynamically transformed so as to follow the rigid-body motion of the seal.This way, the interaction between the ejected seal and the fluid flow can be accurately captured. The second approach simplifies the problem by assuming a quasi-one-dimensional flow (Q1D) in the motor. The nozzle seal rupture is modelled as a gradual opening of the nozzle, with a prescribed characteristic time. We show that both approaches yield nearly identical dynamics on a small-scale test motor, thus validating the use of the cheaper Q1D approach.

Parametric studies in Q1D show that there exists a threshold value of the characteristic rupture time, below which the internal dynamics is identical to that obtained when assuming an instantaneous opening of the seal. For longer rupture times, the intensity of the expansion wave may be greatly reduced.

DOI: 10.13009/EUCASS2023-557

2. 3D simulations with overlapping meshes

In this section, we focus on the simulation of the seal rupture transient using a geometrically-accurate 3D representation of the flow and nozzle. There are instances where the seal is constructed in such a way that it fragments upon rupture, releasing multiple debris which are ejected in the nozzle. Some other seals instead are designed so that the rupture occurs along the nozzle contour, thus producing a single circular fragment that remains in one single piece during ejection. The former is complex to accurately represent in 3D simulation, since dynamic fragmentation requires a well-calibrated model of the seal mechanics. Also, the number of fragments evolves during the rupture, which may be cumbersome to handle numerically. Instead, we choose to focus only the latter case, where the seal remains as a single piece.

2.1 Principle

We study the small experimental motor LP13 from ONERA [6], which is an axisymmetric motor whose geometrical profile is represented in Figure 1. The initial position of the seal is marked in red. The combustion chamber and the nozzle is meshed in 3D. A rectangular mesh extension with gradual mesh coarsening is added after the nozzle exit plane. The nozzle seal is meshed separately. It is a simple steel cylinder 0.25 mm thick and with a radius of 12.15 mm. Its mass is 0.9 g. A simple prism-layer mesh is generated around it.

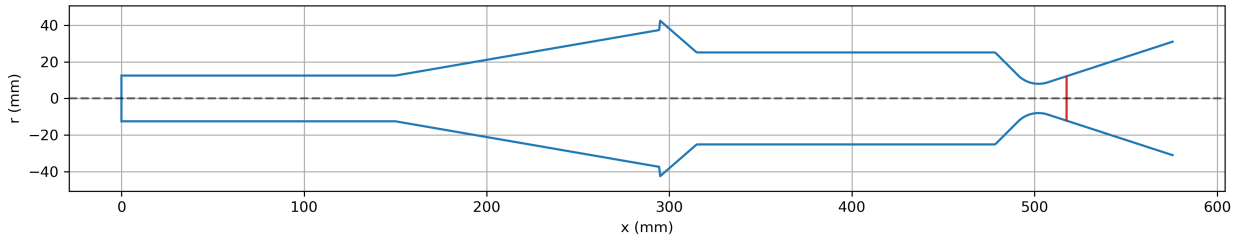

Figure 1: Profile of the axisymmetric LP13 motor

In the CFD toolchain Cedre from ONERA, the "Maillages Chevauchants Conservatifs" module (MCC, overlapping conservative meshes) enables to dynamically cut the motor mesh (background mesh) with the seal mesh, based on the position of the seal. Dynamic connectivities between both meshes are generated, so that the CFD solver Charme of Cedre can simulate the fluid flow around the dynamically moving seal. This way, a global fluid mesh can be constructed, in which the boundary of the seal is accurately represented. The movement of the seal is computed assuming a rigid-body motion, using the pressure and viscous stress distribution computed at its surface. To ensure an accurate result, the mesh intersection algorithm is executed at every time step. A mesh configuration extracted from one of the computations presented further in this article is shown in Figure 2.

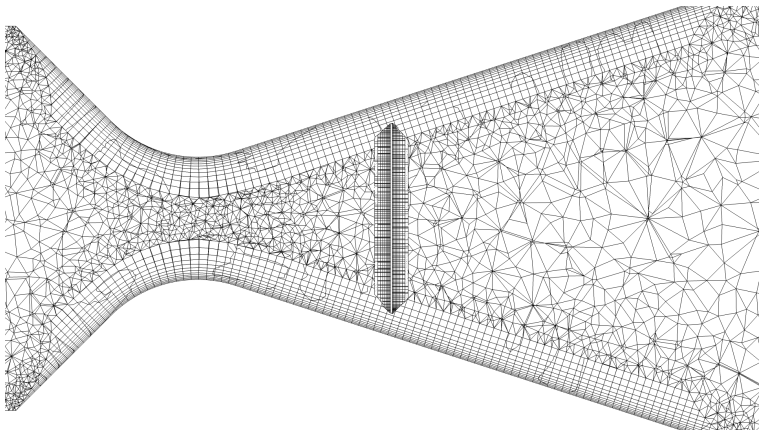

Figure 2: Intersection of the seal and background meshes

To simplify our simulations, we do not consider the ignition and burning of a propellant load inside the motor. Instead, we assume the inner boundaries of the motor are all adiabatic no-slip walls, and we impose a uniform initial

DOI: 10.13009/EUCASS2023-557

internal pressure representative of the seal rupture pressure. The velocity field is initialised at zero and the temperature is set to 300 K. This choice of temperature is intended for comparison with cold-gas experiments currently undergoing at ONERA, which will not be discussed further. The outer fluid is initialised similarly, except for its pressure which is set to 1 bar. The boundary conditions of the mesh extension are subsonic outlets, with a prescribed pressure of 1 bar. We assume the seal ruptures instantaneously from the nozzle, hence it is allowed free movement directly after initialisation.

The gas is simply taken as air, modelled as a single perfect gas with properties representative of ambient temperature. Its Laplace coefficient is $\gamma = 1.4$, the molar mass is $\mathscr{M} = 29$ g/mol, and the specific heat is $c_p = \gamma(R/\mathscr{M})/(\gamma-1) = 1003.4$ K/kg/K, with $R = 8.314$ J/mol/K the universal gas constant. The fluid flow is modelled with the Navier-Stokes equations.

Simulations are carried out in two steps. First, we compute the initial ejection transient from $t = 0$ onwards, until the seal is 6 cm away from its initial position, ensuring that it has no longer an effect on the internal flow field. Indeed, the nozzle throat is already choked at that point. With a seal mass $m = 0.9$ g, this corresponds to $t = 0.5$ ms. The simulation is then continued, but the MCC module is deactivated and the seal mesh is removed, i.e. we only simulate the fluid flow on the original background mesh. The evolution of the complex wave structure in the chamber can then be simulated at a much lower computational cost.

Both steps are carried out with a CFD time step $\Delta t = 1 \times 10^{-7}$ s. The fluid flow model is semi-discretised in space with a second-order finite-volume scheme based on MUSCL reconstruction. The dynamic mesh intersection process may produce fine cells which would require a smaller time step to ensure stability with an explicit time marching scheme. Therefore, we use the implicit Euler scheme, in its linearised variant.

2.2 Results

2.2.1 Fluid flow and seal motion

Ejection simulations are carried out with an initial pressure $P = 40$ bar and $P = 80$ bar. Figure 3 shows the pressure field in the nozzle and around the seal at various times, in the case of initial pressure of 40 bar. Figure 4 shows the velocity and Mach field at the latter time. The throat is sonic, and large velocities are attained around the seal.

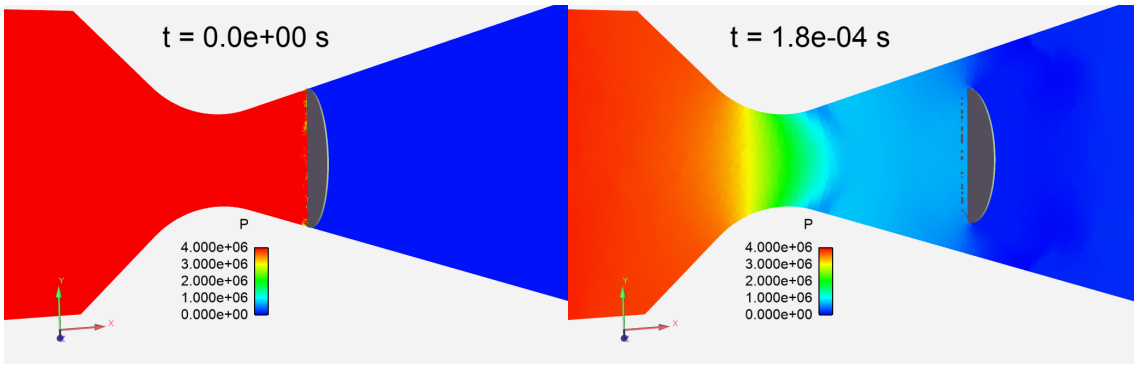

Figure 3: Pressure field and seal movement for $P = 40$ bar

2.2.2 Nozzle seal trajectory

The ejected seal has negligible rotations. Translation most predominantly occurs along the motor axis $\vec{x}$, as expected from the axisymmetric configuration. Figure 5 shows the longitudinal trajectory of the seal for $P = 80$ bar. The initial acceleration is 2×10^5 g. The seal quickly moves away and its speed seems to converge at about 250 m/s.

Two other trajectories are plotted from comparison. The first one correspond to a very simple model where the seal is ejected with a constant acceleration, equal to half of the initial acceleration $\Delta P(t = 0)S/(2m)$, with ΔP denoting the pressure difference between both sides of the seal, and S the seal surface. We see that the initial movement phase is well reproduced, however it quickly diverges away from the true solution. The last curve is obtained by simply recomputing the seal trajectory using the true evolution of ΔP extracted from the CFD simulation. We see that the true movement is excellently reproduced. This verifies the coherence of the trajectory computed by the MCC module, and also shows that viscous forces are negligible.

DOI: 10.13009/EUCASS2023-557

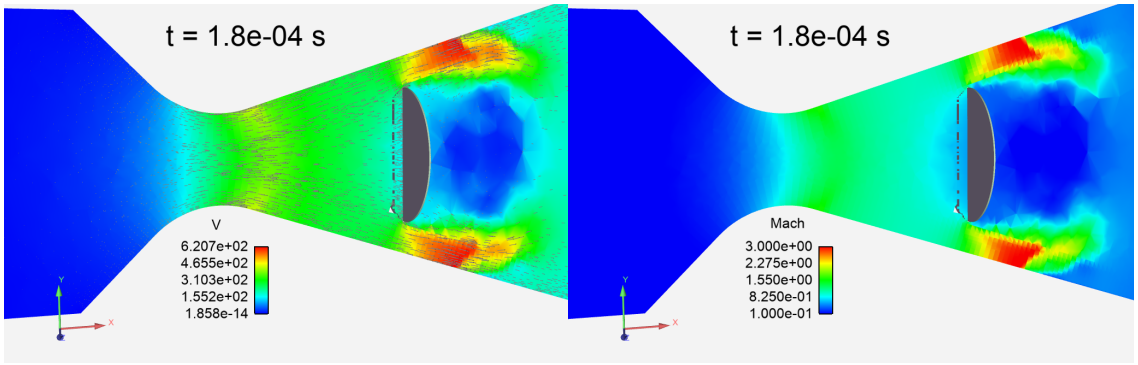

Figure 4: Velocity and Mach field at $t = 0.18$ ms

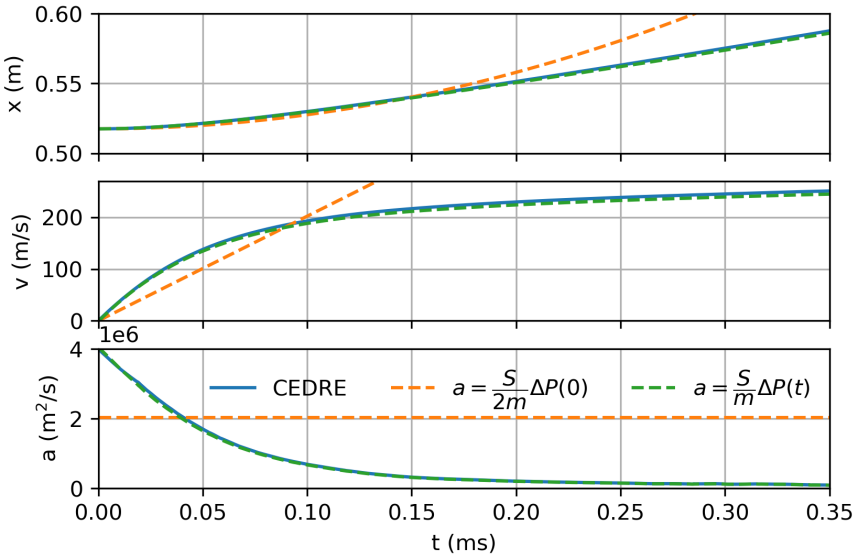

Figure 5: Nozzle seal trajectory for $P = 80$ bar

DOI: 10.13009/EUCASS2023-557

Figure 6 compare the trajectories obtained for $P = 40$ bar and $P = 80$ bar. We observe as expected a doubling of the initial acceleration. However, the seal velocity stabilises on a similar time scale, and the final speed are of the same order of magnitude (200 and 250 m/s).

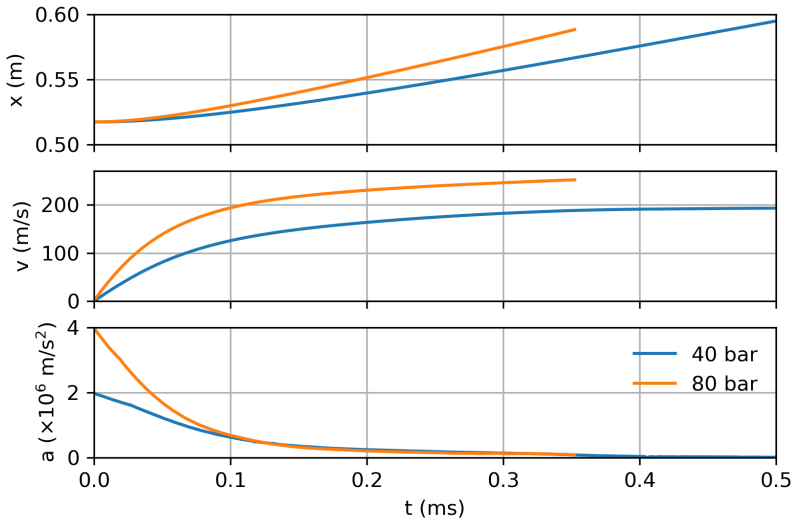

Figure 6: Effect of the initial pressure on the longitudinal trajectory

2.2.3 Internal pressure waves

Our initial aim is to study the effect of a non-instantaneous nozzle seal ejection on the internal ballistics of the motor. To determine the impact of the seal inertia, additional CFD computations are carried out for both pressure levels, without accounting for the seal, i.e. as if it was instantaneously removed.

Figure 7 compares the pressure evolutions obtained at the fore-end of the motor. We observe that accounting for the seal movement has a very negligible effect. The seal is simply ejected far too quickly to have a noteworthy impact on the internal dynamics. This will be further investigated in Section 5. Additionally, the amplitude of the pressure oscillation seems to be direclty proportional to the initial pressure. This will be further discussed in Section 4.1.

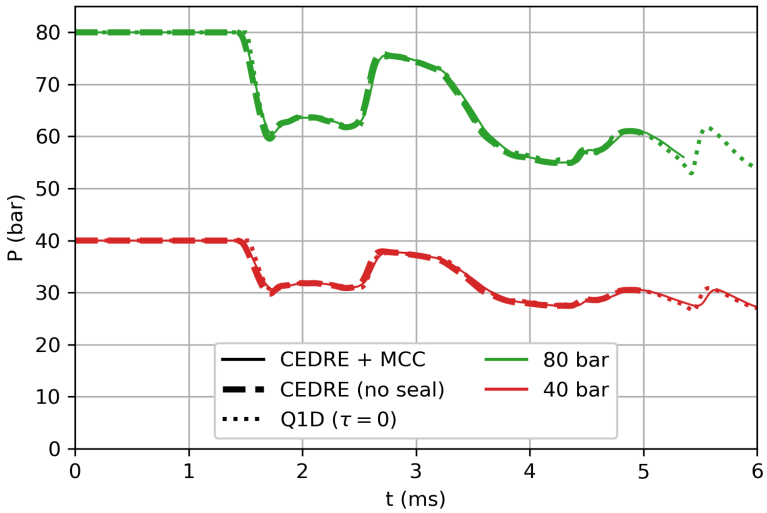

Figure 7: Pressure at the fore-end of the motor

DOI: 10.13009/EUCASS2023-557

3. Simplified quasi-one-dimensional approach

The previous simulation strategy is well suited when the seal remains in one piece. This is however not always the case, as it often happens that the seal may first tear down before breaking in multiple chunks. Simulating such a complex phenomenon is difficult (large deformations, evolving topology) and cannot be done with the previous approach. Also the cost associated with the 3D CFD computation and the mesh intersection algorithm is large.

A simpler approach can be envisioned. The flow in the motor and nozzle being predominantly longitudinal (along $\vec{x}$) in such elongated motors, it is tempting to use a simpler quasi-one-dimensional (Q1D) compressible flow model to represent its dynamics. In this model, multi-dimensional effects only appear through a space-variation of the cross-section available for the flow to pass through. In the original 3D framework, the Euler equations read:

$$\begin{cases} \partial_t \rho + \nabla \cdot \rho\vec{u} = 0 \\ \partial_t \rho\vec{u} + \nabla \cdot (P + \rho\vec{u} \otimes \vec{u}) = 0 \\ \partial_t \rho E + \nabla \cdot \rho\vec{u} h_t = 0 \end{cases} \tag{1}$$

with $E = c_v T + \frac{1}{2}\|\vec{u}\|^2$ the total volumetric energy, and $h_t = E + P/\rho$ the total enthalpy.

Assuming that $\vec{u} = u \cdot \vec{x}$ and that all scalar variables only depend x, we can integrate in space along $\vec{y}$ and $\vec{z}$ over the cross-section (surface $A(x)$) to obtain the following Q1D system:

$$\begin{cases} \partial_t(\rho A) + \partial_x(\rho u A) = 0 \\ \partial_t(\rho A u) + \partial_x\left((P + \rho u^2)A\right) = P d_x A \\ \partial_t(\rho A E) + \partial_x(\rho u E A) = 0 \end{cases} \tag{2}$$

This Q1D formulation is the most conservative one, since only a single term cannot be cast in divergence form. Note that, for solid rocket motors, it is straightforward to add source terms representing the mass and energy injection due to the propellant combustion[7].

3.1 Numerical scheme

We semi-discretise the previous Q1D system in space with a cell-centered finite-volume scheme [8]. A second-order MUSCL-type scheme is used for the convective terms, while the non-conservative term is approximated via centered finite-differences. A minmod limiter is used to ensure the total-variation-diminishing property of the solution. A flux-vector splitting approximate Riemann solver is used to compute the fluxes at the cell boundaries. For the i-th cell (located between the faces $i \pm \frac{1}{2}$), the convective part is discretised as:

$$V_i d_t Q_i = A_{i-\frac{1}{2}} F(Q^-_{i-\frac{1}{2}}, Q^+_{i-\frac{1}{2}}) - A_{i+\frac{1}{2}} F(Q^-_{i+\frac{1}{2}}, Q^+_{i+\frac{1}{2}}) \tag{3}$$

where $Q = (\rho A, \rho A u, \rho A E)^t$, V_i is the volume of the cone joining the faces $i - \frac{1}{2}$ and $i + \frac{1}{2}$, i.e. the volume the i-th cell represents in 3D. The left- and right-reconstructed states $Q^{\pm}_{i\pm1/2}$ are obtained with the MUSCL-reconstruction and limitation, while F is the operator associated to the approximate Riemann solver for the computation of fluxes.

Other discretisations of alternative non-conservative formulations have been implemented [7], however they where less robust to abrupt cross-section variations, hence they will not be discussed further.

3.1.1 Accounting for the nozzle seal

Within our Q1D framework, it is difficult to account for the seal movement during its ejection. Indeed, the complex flow around the seal cannot be accurately captured in 1D. Hence, we propose to account for the seal rupture in an idealised manner, where the seal does not move but is gradually removed. Let us denote its longitudinal position as x_s, where the unsealed cross-section is $A_{max} = A(x_s)$ as described by the geometry of the nozzle. We choose an *a priori* characteristic rupture time τ and we impose that the cross-section available for the flow to pass through at the seal location is $A_s(t)$, defined as:

$$\begin{cases} A_s(t) = 0 & t < 0 \\ A_s(t) = A(x_s)\dfrac{t}{\tau} & 0 < t < \tau \\ A_s(t) = A(x_s) & t > \tau \end{cases} \tag{4}$$

Hence, we assume the cross-section area opens linearly in time. Numerically, we make the seal location x_s coincide with a mesh face. If, for that particular face, we simply replace its equivalent surface by the previous definition of A_s,

DOI: 10.13009/EUCASS2023-557

we will obtain a very steep gradient $d_x A$ locally, which will generate unphysical pressure fluctuations. Also, such a procedure does not behave well in the case where $A_s = 0$, since it is not able to reproduce a reflection of the flow onto the unruptured seal.

We propose instead to split the computational domain at the seal location in two blocks: the inner motor, and the divergent. Both domains are connected through the gradually disappearing seal. However, the cross-section A which appears in the Q1D equations is set to its unsealed value $A(x_s)$ for the mesh face located at the seal position between both domains. At the seal mesh face, convective fluxes are computed with the Riemann solver, assuming an unsealed cross-section. We also compute the convective fluxes that would be obtained if the seal were considered as a wall (i.e. reflection condition). The actual fluxes $F_s^{\pm}$ through the seal mesh face are then obtained as a weighted average of the fluxes, with weights depending on the ratio $\alpha = A_s(t)/A(x_s)$ (proportion of the surface that has been unsealed):

$$F_s^- = \alpha F(Q^-, Q^+) + (1-\alpha) F(Q^-, \tilde{Q}^-) \tag{5}$$

$$F_s^+ = \alpha F(Q^-, Q^+) + (1-\alpha) F(Q^+, \tilde{Q}^+) \tag{6}$$

Here Q^- represents the reconstructed conserved variables $(\rho^-, \rho u^-, \rho E^-)$ at the seal mesh face, based on the left domain, while Q_+ represents their reconstructed values based on the right domain. The term $F(Q^-, Q^+)$ is the classic flux vector computed by solving a Riemann problem, as would be used for any other mesh face where no seal is present. It represents the flux that exits the cell upstream of the seal (and enters the downstream cell) if the seal mesh face is unobstructed. The term $\tilde{Q}$ represents the fictitious state $(\rho, -\rho u, \rho E)$ which, when used in conjunction with a Riemann solver, produces a flux corresponding to a reflection of the flow on a wall. Therefore the term $-F(Q^-, \tilde{Q}^-)$ represents the flux that enters the left cell due to a complete reflection of the flow at the seal mesh face. Note that it is not equal to $F(Q^+, \tilde{Q}^+)$.

The present formulation has a more satisfactory behaviour. It is able to account correctly for the cases $A_s = 0$ or $A_s = A(x_s)$, and provides a smooth transition between these two limit cases.

3.1.2 Time discretisation

The space semi-discretisation yields a system of ODEs of the form $d_t Y = f(Y)$, which we integrate in time with a third-order explicit SSP Runge-Kutta method[9]. This improves the stability limit of the numerical solution compared to non-SSP schemes, e.g. RK4, while still ensuring high-order accuracy. The time step is dynamically chosen so that the maximum CFL number is 0.4.

3.2 Validation against the 3D approach

The previous model and discretisation schemes have been implemented in Python. We can compare the results obtained with the Q1D approach and the 3D modelling, with or without accounting for the seal interaction with the flow. In the case of the real nozzle seal (mass $m = 0.9$ g), Figure 7 shows the evolution of the pressure obtained at the fore-end of the motor for an initial pressure of 40 or 80 bar. The Q1D simulations have been performed with $\tau = 0$, i.e. instantaneous seal rupture and ejection, and a uniform mesh of 200 cells.

We observe that the agreement is excellent between the 3D and Q1D results. In particular, the pressure oscillation amplitudes are identical. This validates the Q1D model and its implementation. With this setup, it takes roughly 2 minutes on a single thread to simulate a 10 ms nozzle seal rupture transient in the LP13 configuration, making it affordable to perform large parametric studies. Also, it is easy to study the effect of τ with the Q1D model, which motivates the following section.

4. Parametric study on the characteristic rupture time

In this section, we investigate the effect of the characteristic seal rupture time τ and initial pressure P_0 on the intensity of the pressure waves travelling through the motor after the seal rupture. We start at $t = 0$ with a sealed nozzle, and we apply the same initialisation as for the 3D simulation presented in Section 2. We test various opening times from $\tau = 0$ to $\tau = 10$ ms, and two inner initial pressures, 40 and 80 bar. Each simulation is run for a physical time of $t_f = 10$ ms, so that the pressure waves can travel multiple times through the motor.

4.1 Results

Figure 8a shows the pressure evolution obtained at the fore-end of the motor for the various opening times, using $P_0 = 40$ bar. For each of the simulation, this signal is filtered with a high-pass fifth-order Butterworth filter with a

DOI: 10.13009/EUCASS2023-557

cut-off frequency of 250 Hz to extract the pressure oscillation, removing the slow average pressure decay. The filtering is executed once in forward time and once in backward time (with the function `signal.sosfiltfilt` from Scipy) so that no phase change is introduced. The obtained filtered pressures are plotted in Figure 8b.

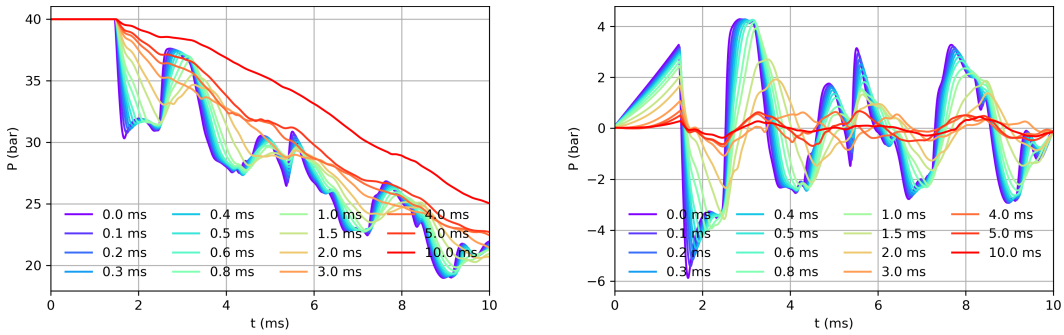

(a) Original signal

(b) Filtered signal

Figure 8: Fore-end pressure in Q1D for $P_0 = 40$ bar

We see that the pressure oscillations decrease when τ increases, but only if τ is above a certain threshold, which here seems to be around $\tau = 0.5$ ms. To quantify this behaviour, the amplitude of the pressure wave is determined in two ways. A first solution is to consider the gap between the extrema of the filtered signal, while a second one is to take its RMS level:

$$P_{RMS} = 2\sqrt{2}\frac{1}{t_f}\sqrt{\int_0^{t_f} \tilde{P}^2 dt} \tag{7}$$

which yields an average amplitude accounting for the gradual decay of the oscillation. Figure 9a shows the evolution of the extracted amplitudes as a function of τ, with a logarithmic scale for τ. In Figure 9b we use a linear scale for τ and we rescale all the curves so that their values at $\tau = 0$ is 1.

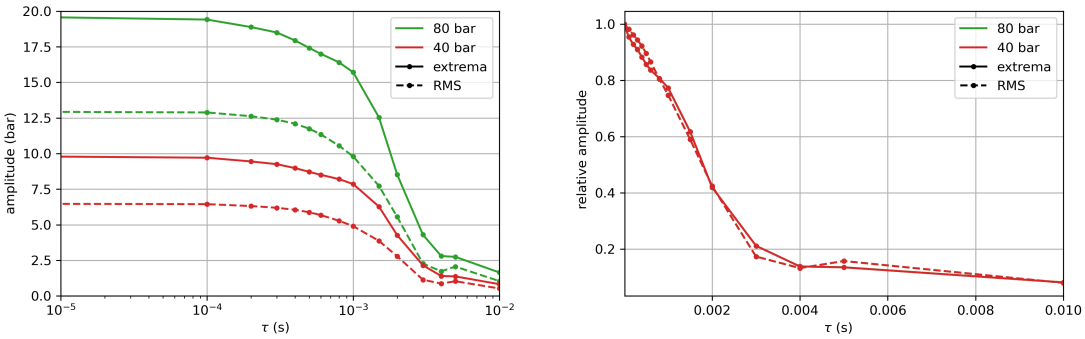

(a) unscaled

(b) scaled based on the amplitude obtained for $T = 0$

Figure 9: Amplitude of the pressure oscillation at the fore-end of the motor

An interesting remark is that, for the rescaled curves, the results for both initial pressures exactly overlap, i.e. no nonlinear effect related to the absolute pressure level is found. Although not shown here, this has also been observed for the unsteady pressure signals. With Figure 9a, we see that when the seal ruptures too quickly ($\tau < 0.5$ ms), the effect of τ on the amplitude is negligible. On the other side of the spectrum, when the characteristic time is long ($\tau > 3$ ms), the effect of a variation in τ is also negligible and the amplitude converges to zero for $\tau \to \infty$, as we would expect from a physical point of view. However, in-between these two regimes the amplitude strongly depends on τ. Using the linear scale Figure 9b, we see that the amplitude A_p is linear in τ:

$$A_p(P_0, \tau) \approx A_p(P_0, 0)\,(1 - 300\tau) \tag{8}$$

Therefore, a 50 % decrease of the pressure oscillation amplitude (compare to the case of an instantaneous rupture) is obtained for $\tau = 1.7$ ms. Of course, this value will depend on the configuration and on the operating conditions.

DOI: 10.13009/EUCASS2023-557

Although not reported in this article, a similar trend with the same regimes has been observed for the effect of τ on the amplitude of the longitudinal pressure delta (difference between fore- and aft-end pressures) and on the value $\max_{x\in[0,480]\text{mm}} P - \min_{x\in[0,480]\text{mm}} P$, which represents the instantaneous maximum longitudinal pressure difference in the motor. This means that the longitudinal pressure gradient also diminishes linearly with τ, up to the regime $\tau > 3$ ms, where it becomes very low and asymptotically converges to zero.

Both the longitudinal pressure difference and the amplitude of the pressure field oscillation at any point in the motor are of importance with respect to the structural loading of the motor. This parametric study in Q1D shows that the nozzle seal rupture time may lead to a dampening of this loading.

4.2 Nozzle throat chocking

From a physical point of view, it is expected that the dynamics of the seal ejection does no longer impact the internal flow field once the throat has become choked. Indeed, perturbations generated by the seal in the divergent are carried out with the supersonic flow towards the nozzle exit plane. It is therefore instructive to investigate the evolution of the throat Mach number in our simulations, as reported in Figure 10 for the various values of τ. We observe that the time t_M required to reach a sonic throat increases with τ. Studying the evolution of t_M with τ has revealed that it is an affine function of τ, i.e. the effect of τ is linear.

Here, we have only shown the curves for $P_0 = 40$ bar. It is interesting to note that the curves are identical for $P_0 = 80$ bar. Although surprising at first, this can also be found in the analytical solution for a simple 1D shock tube[10]. In this configuration, the solution upstream of and at the position of the initial initial pressure discontinuity is described solely by the left initial state and, in particular, the original left pressure level does not impact the value of the Mach number field in that region.

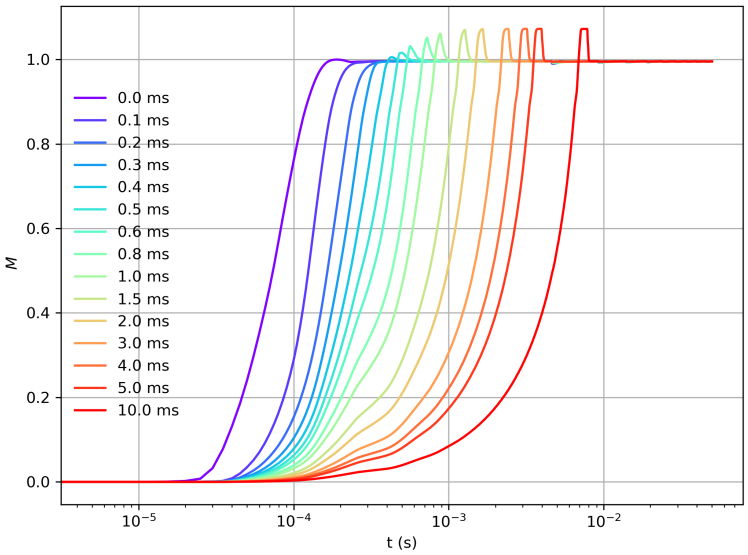

Figure 10: Throat Mach number evolution for various characteristic times τ

5. Comparison of both approaches

Our previous parametric study in Q1D suggested that the characteristic seal rupture and ejection time must be on the order of 1 ms to have a noticeable impact on the internal pressure waves. We now turn back to the 3D simulation framework from Section 2 to see how a longer ejection time can be obtained. Our approach is to artificially weigh the seal down in the MCC module to obtain a slower ejection. We run the 3D simulations again with $m = 0.9$ g, $m = 9$ g, $m = 45$ g and focus on the case of $P = 80$ bar. We also compare the results obtained to those of the Q1D approach with various values of τ.

DOI: 10.13009/EUCASS2023-557

5.1 Results for $m = 0.9$ g

This case has already been treated in Section 3.2. The Q1D and 3D approaches are in good agreement, and accounting for the seal ejection in 3D with the MCC module does not have a noticeable effect on the internal pressure fluctuations. Figure 11 provides a comparison of the throat Mach number obtained with the various modelling strategies. As already discussed, Q1D simulations at 40 and 80 bar produce identical evolutions. The same is true for the 3D simulations from Cedre without accounting for the nozzle seal. If the MCC module is activated to track the seal during its ejection, the chocking of the nozzle is slowed down, and this time an effect of the initial pressure is visible: the throat is more quickly choked for a higher initial pressure, since the seal is ejected more quickly. The physical times required to reached a choked condition (roughly 0.15 to 0.25 ms) remain low enough compared to the characteristic time $\tau = 0.5$ ms that the parametric study in Q1D showed to be the limit value below which no effect on the internal pressure waves. This is consistent with our observations in the 3D simulations, with or without seal.

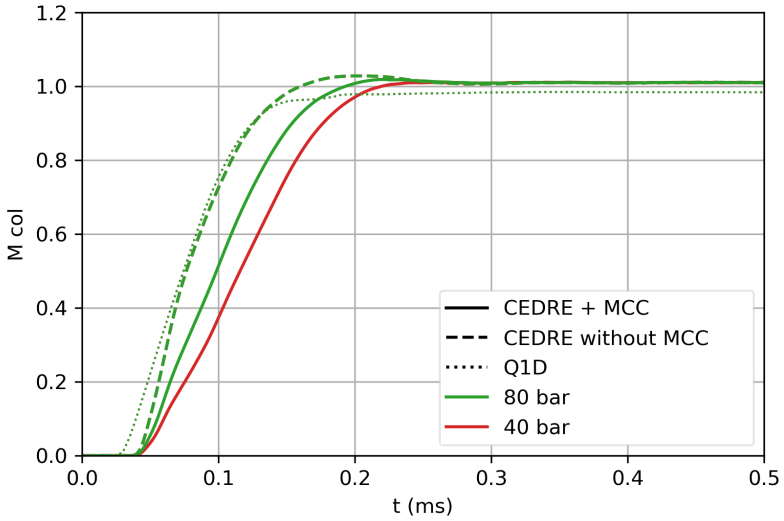

Figure 11: Throat Mach number

5.2 Results with a heavier seal

Figure 12 compares the trajectory of the seal in the 3 cases ($m = 0.9$, 9 and 45g). The initial accelerations are logically inversely proportional to m. The terminal speeds are quite different : the seal reaches 250 m/s for $m = 0.9$ g, 110 m/s for $m = 9$ g, and 50 m/s for $m = 45$ g.

Figure 13 presents the comparison of the pressure evolutions at the fore-end of the motor. Q1D results obtained with manually selected values of τ have also been included. We see that the increased seal masses have a softening effect on the pressure evolution, however they do not impact the amplitude of the oscillation overall. Q1D simulations are in very good agreement with the 3D results, which allows for an *a posteriori* determination of an equivalence between the seal mass m and the corresponding Q1D characteristic seal opening time τ. For a seal of mass $m = 0.9$ g (respectively 9 and 45 g), the equivalent values of τ is 0 ms (respectively 0.4 and 0.8 ms).

Extrapolating this equivalence to larger values of τ shows that is physically impossible to reach the second regime ($\tau \approx 1$ ms) identified in our Q1D parametric study (see Figure 9) if the sole mechanism that can slow the seal ejection is its inertia. Note that characteristic times observed experimentally on the LP13 motor are closer to 0.15 ms. Hence, for this particular configuration, our results show that a detailed modelling of the seal ejection is not useful: simply using a wall condition for the seal and letting it disappear instantly once the seal breaking pressure is reached will be sufficiently accurate.

6. Conclusion

In this article, we have presented two modelling approaches to study the ejection of a nozzle seal during the ignition phase of a rocket motor. The first approach, based on a detailed geometrical representation of the seal in 3D, provides a

DOI: 10.13009/EUCASS2023-557

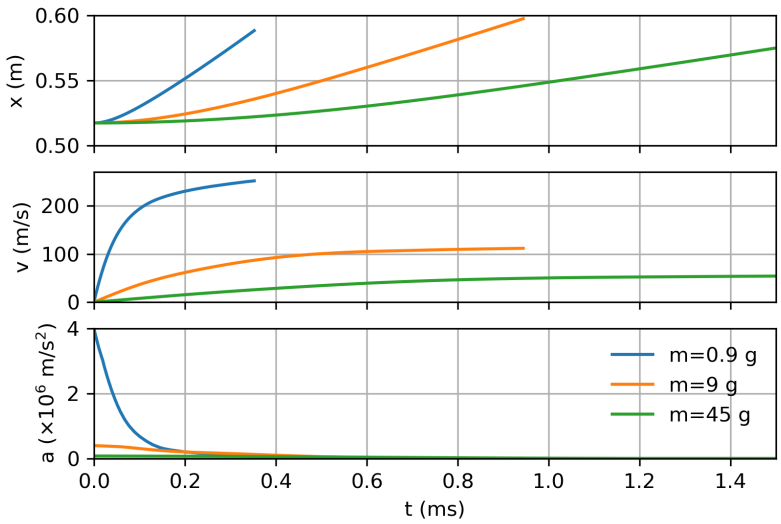

Figure 12: Seal trajectories with various masses for P_0 = 80 bar

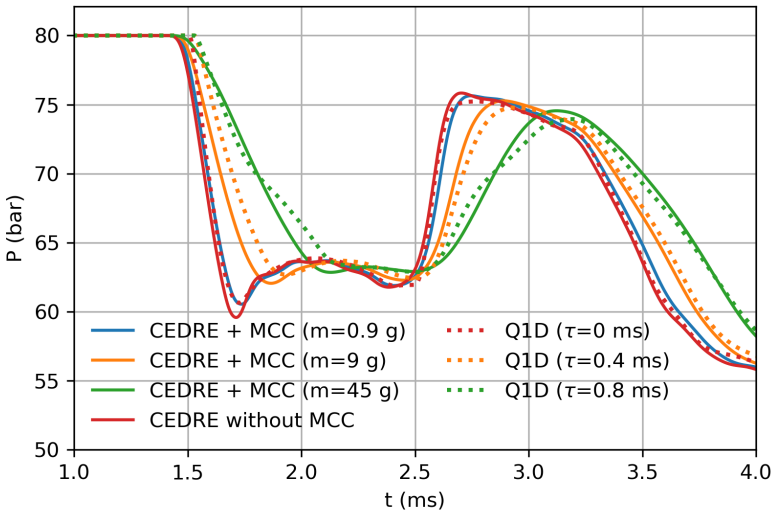

Figure 13: Fore-end pressure for various seal masses

DOI: 10.13009/EUCASS2023-557

reference computation that makes it possible to simulate the trajectory of the seal during ejection. The second approach largely simplifies the modelling by assuming a quasi-one-dimensional flow in the motor. The gradual ejection of the seal is represented as a progressive opening of the passage area initially obstructed by the seal. Since the seal dynamics is not modelled, an *ad hoc* prescription of the characteristic seal ejection time τ is required. Comparisons between both approaches have validated the simplified modelling.

Using the cost-effective Q1D approach, extensive parametric studies can be carried out. Investigations have shown that the initial pressure level has only a scaling effect on the amplitude of the pressure oscillations that occur inside the motor after the seal is ruptured. Regarding the effect of the characteristic time τ of the seal ejection, 3 regimes have been identified. For very low values of τ, the amplitude is the same as for $\tau = 0$. For $\tau > 3$ ms, a value which will depend on the studied configuration, the amplitude is very low, and in the limit $\tau \to \infty$, it converges to zero. In-between these two regimes, an intermediate zone has been identified, where the amplitude decreases linearly with τ.

A comparison has been made between the Q1D and 3D approaches for artificially increased seal masses m. It is possible to build an equivalence between m and τ by matching the Q1D results to the 3D ones. For the studied configuration, the second regime cannot be reached with realistic seals, since the equivalent value of τ remains well within the first regime for any reasonable value of the seal mass. Thus, the dynamics of the seal ejection have no noticeable effect on the internal pressure waves generated by the seal rupture.

In light of the work presented here, it can be assumed that the three regimes identified in Q1D are generic and can be found for any motor. The issue of practical importance is then to determine the values of τ that separate the three regimes for a given configuration. Future work will apply the Q1D methodology to other motors, in particular larger ones, to identify how the change in geometry and operating conditions affect these findings. Theoretical investigations should also be conducted to determine the variables (e.g. temperature, geometrical parameters) which have an effect on these regimes. Finally, experiments on small scale motors are being performed at ONERA and will provide valuable information for the validation of our numerical findings.

7. Acknowledgments

This work has been conducted in the framework of a study funded by AID - French Ministry of Defence. The author would like to thank P. Grenard for his help with the MCC module of Cedre.

References

[1] W.A. Johnston. Solid rocket motor internal flow during ignition. *Journal of Propulsion and Power*, 11(3):489–496, 1995.

[2] P. Le Helley. 3D turbulent Navier-Stokes simulations of ignition transients in solid rocket motors. In *34th AIAA/ASME/SAE/ASSE Joint Propulsion Conference and Exhibit*, 1998.

[3] P. Brenner. Three-dimensional aerodynamics with moving bodies applied to solid propellant. In *27th Joint Propulsion Conference*, page 2304, 1991.

[4] Alexandre Limare, Pierre Brenner, and Houman Borouchaki. An adaptive remeshing strategy for unsteady aerodynamics applications. In *46th AIAA Fluid Dynamics Conference*, page 3180, 2016.

[5] A. Refloch, B. Courbet, A. Murrone, P. Villedieu, C. Laurent, P. Gilbank, J. Troyes, L. Tessé, G. Chaineray, J.-B. Dargaud, E. Quémerais, and F. Vuillot. Cedre software. *AerospaceLab Journal*, pages 1–10, 2011.

[6] Y. Fabignon, J. Anthoine, D. Davidenko, R. Devillers, J. Dupays, D. Gueyffier, J. Hijlkema, N. Lupoglazoff, J.-M. Lamet, L. Tessé, A. Guy, and C. Erades. Recent advances in research on solid rocket propulsion. *Aerospace Lab Journal*, 11:1–15, 2016.

[7] V. Kalyana Chakravarthy, A.S. Iyer, and D. Chakraborty. Quasi-one-dimensional modeling of internal ballistics and axial acoustics in solid rocket motors. *Journal of Propulsion and Power*, 32(4):882–891, 2016.

[8] E.F. Toro. *Riemann solvers and numerical methods for fluid dynamics: a practical introduction*. Springer Science & Business Media, 2013.

[9] D.I. Ketcheson, C.B. Macdonald, and S. Gottlieb. Optimal implicit strong stability preserving Runge-Kutta methods. *Applied Numerical Mathematics*, 59(2):373–392, 2009.

[10] M. Salita. Closed-form analytical solutions for fluid mechanical, thermochemical, and thermal processes in solid rocket motors. In *34th AIAA/ASME/SAE/ASEE Joint Propulsion Conference and Exhibit*, page 3965, 1998.